TECHNICAL NOTE

In Vivo Assessment and Visualization of Intracranial Arterial Hemodynamics with Flow-Sensitized 4D MR Imaging at 3T

S. Wetzel
S. Meckel
A. Frydrychowicz
L. Bonati
E.-W. Radue
K. Scheffler
J. Hennig
M. Markl

SUMMARY: We evaluated electrocardiogram-synchronized flow-sensitized 4-dimensional MR imaging at 3T in combination with advanced 3D visualization strategies to ascertain its feasibility for the assessment of local intracranial blood-flow patterns in vivo. In large arteries of healthy volunteers, the temporal and spatial evolution of blood flow was successfully visualized and revealed—for example, a helical flow pattern in the carotid siphon. In a patient with steno-occlusive neurovascular disease, stagnant and retrograde flow patterns were readily visible.

The study of local hemodynamics within anatomically complex regions of the human neurovascular system is of high interest because these sites are predisposed to vascular disease such as atherosclerosis and aneurysm formation. Most investigations focusing on a detailed temporal and spatial description of intracranial vascular hemodynamics have been conducted in vitro, using computer models.[1-3] Even if boundary conditions are derived from real patient data, these approaches are still limited by an incomplete description of hemodynamics (2-phase fluid dynamics, non-Newtonian behavior, elasticity and motion of vessel walls, and so forth). Quantitative in vivo assessment of intracranial flow dynamics is possible with ultrasonography techniques which, however, are limited by sound propagation problems in the presence of bone or air cavities. Moreover, flow velocities can only be obtained at discrete regions. Assessment and evaluation of intracranial blood flow in vivo with phase-contrast MR imaging has also been reported but is limited to 2-dimensional (2D) methods and segmental analysis of flow rates.[4,5]

Flow-sensitized 4-dimensional (4D) MR imaging has recently been introduced and combines electrocardiogram (ECG)-synchronized 3D phase-contrast MR imaging with advanced postprocessing strategies for 3D blood-flow visualization. Applications mostly focused on hemodynamics in the heart and great vessels or 3D flow characteristics in model systems.[6-9]

We present the adaptation of 4D MR imaging for the assessment of blood flow in the large intracranial arteries. Different postprocessing techniques were used to illustrate findings in healthy volunteers and in a patient with a proximal carotid occlusion.

Received August 7, 2006; accepted after revision October 16.

From the Department of Medical Radiology (S.W., S.M., E.-W.R.), Institute of Neuroradiology, University Hospital of Basel, Basel, Switzerland; the Department of Diagnostic Radiology (A.F., J.H., M.M.), Medical Physics, University Hospital Freiburg, Freiburg, Germany; the Department of Neurology (L.B.), University Hospital of Basel, Basel, Switzerland; and the Department of Medical Radiology (K.S.), MR-Physics, University Hospital of Basel, Basel, Switzerland.

Please address Correspondence to Michael Markl, PhD, University Hospital Freiburg, Department of Diagnostic Radiology, Medical Physics, Hugstetter Str 55, 79106 Freiburg, Germany; e-mail: michael.markl@iniklinik-freiburg.de

Description of Technique

Volunteers and Patients

Five healthy volunteers (all male; mean age, 29.6 years) and a patient (male, aged 41 years) with occlusion of the left carotid artery as demonstrated by standard MR angiography (MRA) and transcranial Doppler sonography (TCD) were investigated.

The study was approved by the local ethics review committee, and written informed consent was obtained from all subjects.

MR Imaging System and Imaging Parameters

All examinations were performed on a 3T head system (Magnetom Allegra, Siemens, Erlangen, Germany) by using a standard head coil. Flow-sensitized 4D MR imaging consisted of a *k*-space segmented 3D radio-frequency–spoiled gradient-echo sequence with prospective ECG-gating and interleaved 3-directional velocity-encoding. Data acquisition resulted in a series of 3D volumes representing 3D blood flow in consecutive timeframes within the cardiac cycle with a temporal resolution of 54.4–56.0 ms.[8] Further imaging parameters were as follows: $\alpha = 15°$, velocity-encoding value (VENC) = 80–100 cm/s, TE = 4.0–4.4 ms, TR = 6.8–7.0 ms, band width = 450 Hz/pixel.

Flow-sensitive 4D MR imaging was performed in 3 volunteers by using an axial 3D slab to cover the circle of Willis (rectangular FOV = [220 × 165–183] mm^2) with 24–32 sections/slab and a spatial resolution of 1.2 × 1.5 × 1.4–1.5 mm^3. Two additional volunteer scans were performed in midline sagittal orientation with 32 sections/slab, a FOV of 220 × 220 mm^2, and a spatial resolution of 1.2 × 1.5 × 1.5 mm^3.

Postprocessing and 3D Visualization

Noise masking was performed by thresholding of the signal intensity in the magnitude data to exclude regions with low signal intensity such as air or the ventricular system. Further noise reduction and separation of static tissue and vessels were achieved by comparing the standard deviation of the velocity-time course for each pixel in the 4D dataset as described by Buonocore.[10] All preprocessing steps were integrated into a homemade software tool. A built-in preview function permitted the interactive adjustment of thresholds for optimal noise and background suppression.

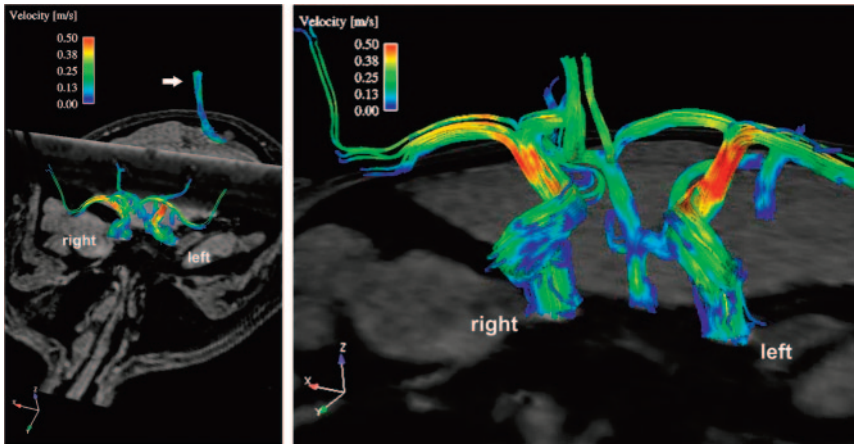

Fig 1. Normal 3D blood-flow patterns and velocities of the circle of Willis by using 3D streamline visualization reveal complex flow patterns and segmental changes in absolute blood-flow velocities (color-coding indicates local blood flow velocity magnitude). Additional streamline visualization was performed in a short segment of the superior sagittal sinus transecting the axial 3D volume (top left, *white arrow*).

Anatomy, blood flow, and vascular geometry included in the resulting data were then visualized by using a 3D software package (EnSight; CEI, Apex, NC). To display anatomic information and to aid data navigation, we automatically reformatted the acquired magnitude data onto 2D planes transecting the 3D data volumes at freely selectable locations and tilt angles (eg, transverse and coronal planes in Fig 1). Different 3D visualization tools were used to depict the spatial and temporal distribution of blood flow within the prescribed 3D data volume. 3D streamline visualization was based on a user-selected frame within the cardiac cycle of the flow-sensitive 4D MR data acquisition. The resulting traces thus represented flow patterns within a temporal window of 55 ms. For all subjects, the timeframe representing peak systole was selected, (ie, with the highest velocities as visually assessed from the color-coded tracings). Time-resolved 3D particle traces resembled the path of virtual massless particles released within the time-varying blood flow velocities, thus illustrating the temporal evolution of blood flow in 3D.[6,10,11]

Consensus image evaluation by 2 experienced readers was performed by using the 4D viewing capability of the visualization software. For particle traces, the data could be displayed in movie mode to permit the visual inspection of the dynamics of 3D flow patterns in interactively selectable view angles.

For axial coverage, all healthy volunteers were visually examined with respect to flow patterns in the distal internal carotid artery (ICA), the circle of Willis, and its proximal branches. For sagittal coverage, image analysis focused on the ICA and the carotid siphon.

TCD

In 2 volunteers, bilateral peak systolic flow velocities were recorded from Doppler frequency spectra in the M1 segment of the middle cerebral artery, the C1 segment of the intracranial ICA, and the A1 segment of the anterior cerebral artery, with correction of the angle between the vascular axis and the sonography beam.

Peak systolic velocities were compared with MR velocity data by using time-resolved 3D particle trace visualization. MR velocities in corresponding vascular segments (A1, M1, and C1) were visually assessed by using stepwise different velocity magnitude color-coding to identify regions with peak flow.

Bilateral peak systolic flow velocities in cm/s derived from TCD and MR imaging (mean +/− SD)

	Peak Systolic Flow [cm/s]		
Vascular segment	C1	M1	A1
MR imaging	73 +/− 11	71 +/− 11	69 +/− 5
TCD	73 +/− 12	100 +/− 13	116 +/− 53

Note:—TCD indicates transcranial Doppler sonography.

For all subjects, total scanning time was heart rate–dependent and ranged from 15–20 minutes.

Preprocessing (noise filtering, eddy current correction, and data conversion) required approximately 10 minutes. Once the data were loaded into the 3D visualization software package, data navigation and the placement of emitter planes within the 4D datasets were the most time-consuming part of the data-evaluation procedure. The entire processing time for the generation of 3D streamlines and time-resolved 3D particle traces within the circle of Willis was on the order of 45–60 minutes.

Healthy Volunteers

Mean peak systolic velocities derived from MR imaging and TCD in segments C1, M1, and A1 are summarized in the Table. On average, velocities from MR imaging (range, 60–85 cm/s) were reduced by 30.3% compared with TCD (range, 59–178 cm/s). Reliable insonation of the ICA (C1 segment) was not possible in 1 volunteer on either side.

Axial Volume Coverage

Results from 3D visualization of intracranial blood flow by using 3D streamlines for a representative overview of systolic 3D blood-flow characteristics in the entire circle of Willis for 1 volunteer are provided in Fig 1. In this volunteer, the highest flow velocities were observed in the distal ICA. Fig 1 also demonstrates the potential of the method to assess the slower venous flow from the same dataset.

To derive information about changes in vascular hemodynamics with time, the inherent temporal information available from the 4D MR imaging dataset could be used. Visualization results from the remaining 2 volunteers with axial volume coverage are depicted in Fig 2. The inspection of the temporal evolution of virtual particle traces illustrates vascular filling and development of specific flow features such as the complex filling of the ICA. For all volunteers, flow was well

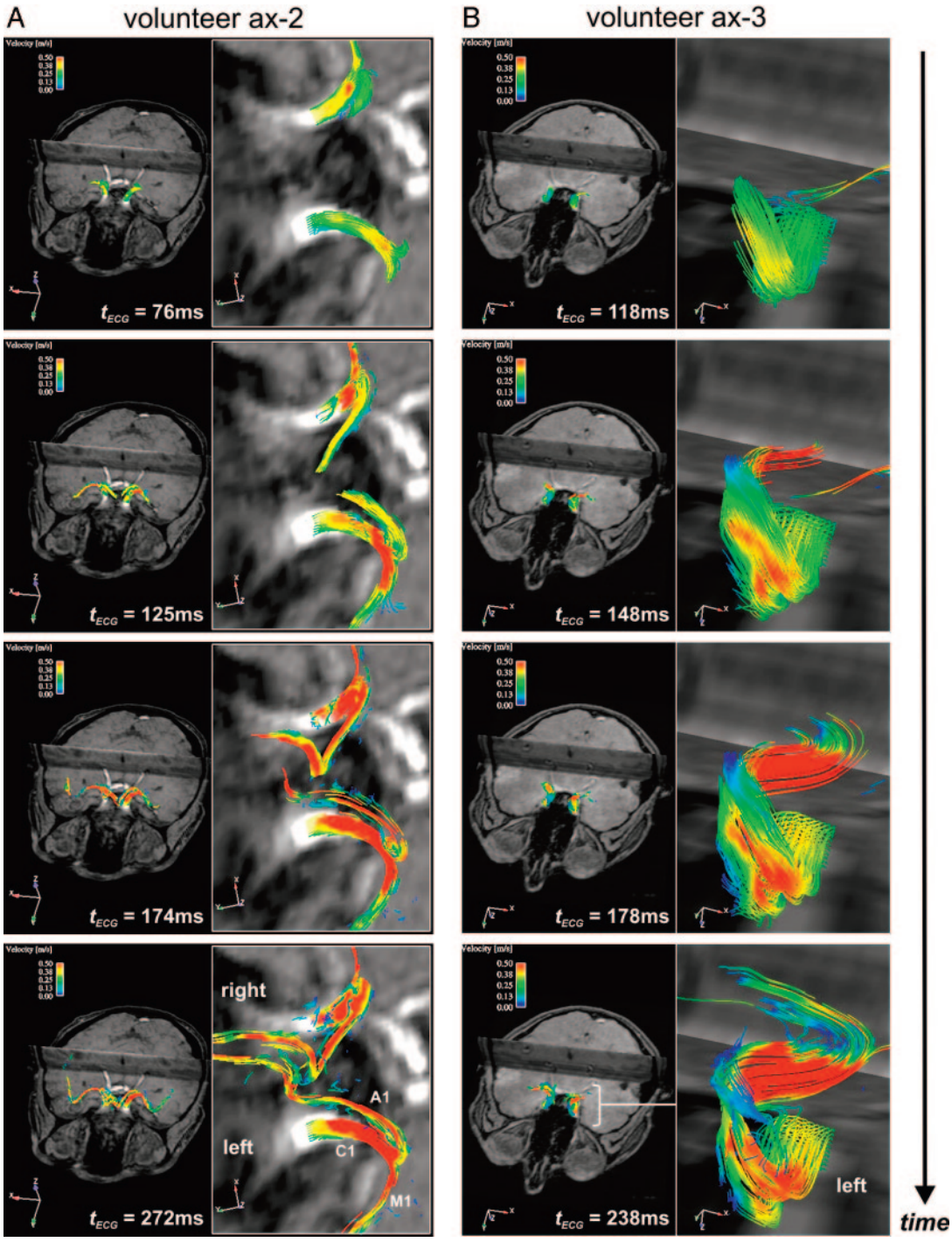

Fig 2. Time-resolved 3D particle traces for 4 successive systolic timeframes illustrating blood flow in parts of the circle of Willis in 2 healthy volunteers with axial (ax) slab orientations. Color-coding corresponds to the local blood-flow velocity magnitude. *A,* Overview of the anterior part of the circle of Willis. Simultaneous systolic filling and local blood-flow characteristics of the left and right C1, M1, and A1 segments can clearly be appreciated. *B,* Targeted view of the left carotid siphon exhibiting complex-flow helical patterns and segmental-flow acceleration.

visualized in left and right C1, M1, and A1 segments. Pulsatile forward flow directed downstream along the anatomic orientation of the vessel was observed in all volunteers. No retrograde flow in any of the inspected segments was seen. One volunteer demonstrated a pronounced helical flow pattern in the carotid siphon (Fig 2*B*).

Sagittal Volume Coverage

Examples from a volunteer are shown in Fig 3 depicting detailed arterial filling of the right carotid siphon. Development of complex helical flow as previously reported in numeric blood-flow simulation studies is clearly visible.[12] Consistent results were obtained in the 2nd volunteer investigated with a targeted sagittal volume (not shown).

Patient

The patient presented with a proximal occlusion of the left carotid artery (LCA), as demonstrated by ultrasonography and 3D time-of-flight MRA (TOF-MRA) (Fig 4). At the level of the carotid siphon, no directional flow was visible on the

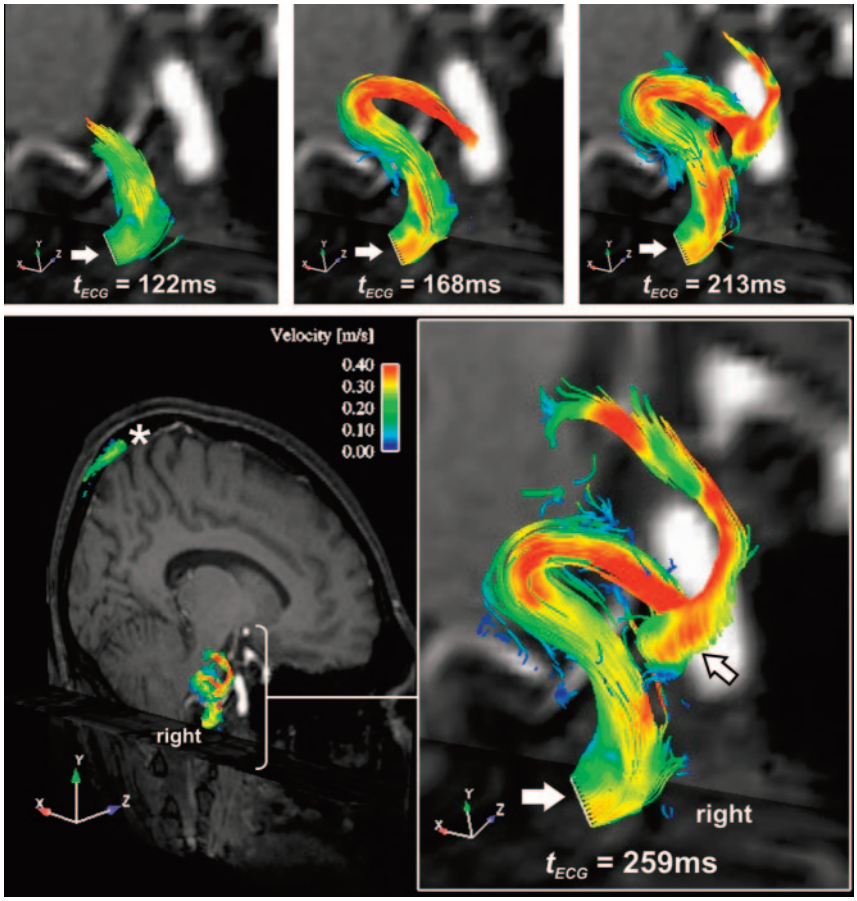

Fig 3. Time-resolved 3D particle traces in 4 consecutive systolic timeframes illustrate the filling of the right carotid siphon. Note the complex and counter-clockwise helical flow pattern (if viewed along the flow direction) in the C5 segment (*open arrow*). The emitter plane from which particle traces were released from equidistant grid points is indicated by the solid white arrow. In the superior sagittal sinus (*asterisk*), particle traces demonstrate lower flow velocities and thus reduced tracer length compared with arterial blood flow.

occluded side, whereas blood-flow patterns and systolic filling on the nonoccluded right side could clearly be identified and appeared normal when compared with volunteer data (Fig 4*B*). In addition, collateral blood flow at the level of the circle of Willis via a small anterior communicating artery, which was also visible in the 3D TOF data (*yellow arrows* in Fig 4*A*), could be visualized successfully (Fig 4*C*, *-D*).

Discussion

The results from volunteer and patient examinations demonstrate the feasibility of flow-sensitized 4D MR imaging for the assessment and visualization of intracranial vascular hemodynamics in vivo.

Compared with sonographic measurements, which is the routine method for a detailed quantitative analysis of cerebral blood dynamics in vivo, 4D MR imaging offers several advantages. First, it is possible to depict 3D velocity fields for a single timeframe with great detail and not merely to measure velocities at discrete points. Complex flow patterns, most notable here a physiologic flow helix at the carotid siphon, can thus be detected. Second, flow measurements are integrated with high-resolution anatomic MR imaging, which provides a detailed topographic allocation of the hemodynamic information obtained. Third, sound propagation problems and angulation errors that are common in sonographic measurements do not pose a problem.

It is thus likely that 4D MR imaging has the potential to contribute to the understanding of neurovascular disease in which disturbed "flow patterns" are regarded as a key element for disease initiation and progression, such as in atherosclerotic disease or cerebral aneurysms. As an example, the detailed in vivo characterization of flow might improve the definition of boundary conditions for 3D computer simulations.[2,13]

The current limitations of the methodology are mainly related to the spatial and temporal resolution and the total scanning time requirement. Although it was possible to visualize crossflow characteristics via a small anterior communicating artery, smaller intracranial vessels could not be detected. Furthermore, the 3D streamlines and particle traces reported in this study did not represent the true underlying spatial resolution but were retrospectively spatially interpolated within the visualization software package. A user-selected number of streamlines and particle traces were extracted from the measured data to improve the flow depictions, similar to zero-filling in MR imaging.

With the given voxel size of $1.2 \times 1.5 \times 1.4$ mm^3 and a cross section of the large intracranial arteries of approximately 10–12 mm^2, only about 10 voxels were placed within the individual vessel. This current resolution, therefore, precludes the determination of important secondary derived flow parameters, such as wall shear stress, because accurate near-wall-velocity gradients could not be obtained. Furthermore, the temporal resolution of approximately 55 ms was relatively low. This might lead to an underestimation of peak velocities due to low-pass filtering. Thus, both spatial and temporal averaging likely contributed to the lower peak velocities that were observed in this preliminary assessment in comparison

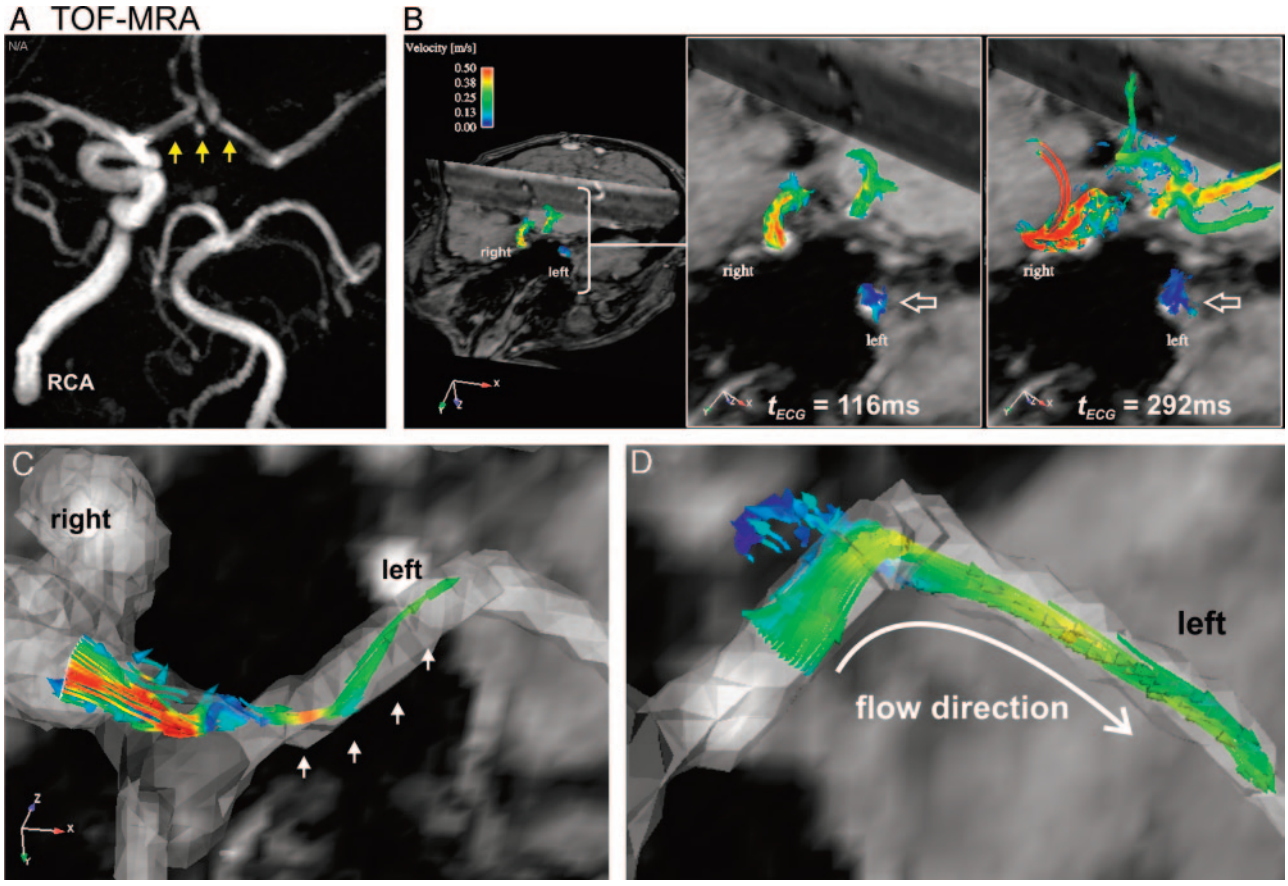

Fig 4. Time-resolved 3D particle trace visualization for a patient with occlusion of the LCA. *A,* TOF-MRA demonstrating occlusion of the LCA and a small anterior communicating artery (*small arrows*). *B,* Arterial filling of the large intracranial vessels for 2 systolic timeframes indicating the absence of flow evolution at the level of the distal left ICA (*open white arrows*). Blood-flow patterns and systolic filling on the nonoccluded right side are clearly visualized. *C* and *D,* Collateral blood flow from right to left via a small anterior communicating artery. *C,* The emitter plane is localized at the right A1 segment. The crossflow via the small anterior communicating artery to the left A1 segment (*arrows*) is clearly visible. *D,* The emitter plane localized in the left A1 segment depicts the retrograde flow direction within that vessel segment.

with TCD; this finding is consistent with previous reports that compared peak velocities from phase-contrast MR imaging and Doppler sonography.[14,15]

Additionally, partial volume effects (ie, voxels containing fractions of arterial lumen as well as surrounding tissue) need to be considered, and they limited the accuracy of the measured velocities. Associated blood-flow-velocity estimation errors or incorrect representation of the size of the vessel lumen or both underline the need for improvements in spatial resolution for accurate evaluation of flow in the small-vessel diameter of the order and below the current pixel size of approximately 2 mm^2.

In this context, the successful visualization of flow through a small communicating artery in 1 patient demonstrated the feasibility for the evaluation of the general flow direction but did not provide detailed information on local flow profiles.

To improve the performance of flow-sensitive 4D MR imaging, one could apply a combination of spatial and temporal imaging acceleration techniques.[16] In the temporal domain, view-sharing (ie, more frequent update of central *k*-space compared with peripheral regions) is expected to provide an improvement in temporal resolution on the order of 30%–40%. Spatial resolution could be enhanced by the application of partial Fourier acquisition and parallel imaging. Assuming partial Fourier factors of 6/8 and parallel imaging with acceleration factors of 2 in both phase and section encoding direction, one might achieve a potential spatial resolution improvement to 0.6–0.8 mm^3 for similar total examination times.[17,18]

However, signal-to-noise ratio (SNR) loss associated with parallel imaging needs to be taken into account and warrants a thorough validation as well as the evaluation of optimal tradeoffs between SNR, spatial resolution, temporal resolution, and total acquisition time in future phantom and human studies.

For flow-sensitized 4D MR imaging, all acquisitions were performed with predefined velocity sensitivity (VENC, 80–100 cm/s), which was selected to exceed to the expected peak velocities in the intracranial arteries to avoid velocity aliasing. Although sonography revealed higher velocities (≤178 cm/s), no velocity aliasing was encountered in the MR images (manual review of all source data before 3D visualization), which might be related to the underestimation of peak velocities by MR imaging but also to the intrinsic variability of sonography.

However, the use of predefined velocity-encoding sensitivities limits the range of blood-flow velocities that can be resolved. Specifically for patients with arterial pathologies such as stenosis, altered vascular geometry can result in substantially accelerated flow, causing velocity aliasing artifacts. Although increasing velocity sensitivity may help to minimize these effects, such a strategy is associated with increased noise

levels in the velocity images, thereby limiting the assessment of slow diastolic or pathologic retrograde flow.

A dynamic adjustment of the VENC with reduced values in the diastolic timeframes in combination with anti-aliasing algorithms such as phase-unwrapping algorithms may thus be suited best to improve the underlying technique.

A further drawback of the implementation used in our study is related to the use of prospective gating for ECG-synchronized data acquisition. As a result, only 80%–90% of the R-R interval could be temporally resolved, so that late diastolic blood-flow velocities could not be assessed. Retrospective gating, as introduced by Pelc et al,[4] would allow the assessment of flow along the entire cardiac cycle without increase in total scanning time.[19]

Further, because of the need to add additional velocity-encoding gradients to the pulse sequence, TE and TR (4 and 6 ms) were increased compared to typical parameters of fast radio-frequency–spoiled gradient-recalled echo (GRE) imaging (approximately 1 and 3 ms). As a result, fast-changing nonconstant flow during such time scales (eg, as complex or turbulent flow in or near stenotic lesions) may result in enhanced signal-intensity loss due to intravoxel dephasing compared with standard GRE techniques. Further improvements in gradient performance and more efficient velocity-encoding strategies in conjunction with systematic studies of signal-intensity characteristics as a function of TE and flow patterns are thus needed to improve the robustness of the method.

For the assessment of arterial vascular structure, contrast-enhanced 3D MRA (3D Ce-MRA) has currently a better spatial resolution and a shorter acquisition time compared with flow-sensitized MR imaging techniques. Further, in time-resolved 3D Ce-MRA, a temporal update rate of 2–3 seconds can be achieved with comparable spatial resolution. Although these techniques permit the assessment of contrast agent dynamics, the ability to resolve 3-directional blood flow over the cardiac cycle with a temporal resolution on the order of tens of milliseconds is not possible. Flow-sensitive MR imaging, on the other hand, exploits the intrinsic sensitivity of MR imaging against movement, in particular blood flow. As a result, large parts of the cardiac cycle can be covered to visualize and quantitatively analyze pulsatile blood-flow patterns at different locations along the arteries.

In conclusion, flow-sensitized 4D MR imaging of the intracranial vasculature is feasible in vivo and can be considered as a promising tool for the assessment of cerebral blood-flow patterns. Improvements and optimization of the technique are required to exploit the information on cerebral hemodynamics that can be derived from this technique.

References

1. Gonzalez CF, Cho YI, Ortega HV, et al. **Intracranial aneurysms: flow analysis of their origin and progression.** *AJNR Am J Neuroradiol* 1992;13:181–88
2. Steinman DA, Milner JS, Norley CJ, et al. **Image-based computational simulation of flow dynamics in a giant intracranial aneurysm.** *AJNR Am J Neuroradiol* 2003;24:559–66
3. Ohta M, Wetzel SG, Dantan P, et al. **Rheological changes after stenting of a cerebral aneurysm: a finite element modeling approach.** *Cardiovasc Intervent Radiol* 2005;28:768–72
4. Pelc NJ, Herfkens RJ, Shimakawa A, et al. **Phase contrast cine magnetic resonance imaging.** *Magn Reson Q* 1991;7:229–54
5. Stock KW, Wetzel SG, Lyrer PA, et al. **Quantification of blood flow in the middle cerebral artery with phase-contrast MR imaging.** *Eur Radiol* 2000;10:1795–800
6. Wigstrom L, Sjoqvist L, Wranne B. **Temporally resolved 3D phase-contrast imaging.** *Magn Reson Med* 1996;36:800–03
7. Kilner PJ, Yang GZ, Wilkes AJ, et al. **Asymmetric redirection of flow through the heart.** *Nature* 2000;404:759–61
8. Markl M, Draney MT, Miller DC, et al. **Time-resolved three-dimensional magnetic resonance velocity mapping of aortic flow in healthy volunteers and patients after valve-sparing aortic root replacement.** *J Thorac Cardiovasc Surg* 2005;130:456–63
9. Isoda H, Hirano M, Takeda H, et al. **Visualization of hemodynamics in a silicon aneurysm model using time-resolved, 3D, phase-contrast MRI.** *AJNR Am J Neuroradiol* 2006;27:1119–22
10. Buonocore MH. **Visualizing blood flow patterns using streamlines, arrows, and particle paths.** *Magn Reson Med* 1998;40:210–26
11. Napel S, Lee DH, Frayne R, et al. **Visualizing three-dimensional flow with simulated streamlines and three-dimensional phase-contrast MR imaging.** *J Magn Reson Imaging* 1992;2:143–53
12. Saloner D, van Tyen R, Dillon WP, et al. **Central intraluminal saturation stripe on MR angiograms of curved vessels: simulation, phantom, and clinical analysis.** *Radiology* 1996;198:733–39
13. Metcalfe RW. **The promise of computational fluid dynamics as a tool for delineating therapeutic options in the treatment of aneurysms.** *AJNR Am J Neuroradiol* 2003;24:553–54
14. Karwatowski SP, Brecker SJ, Yang GZ, et al. **Mitral valve flow measured with cine MR velocity mapping in patients with ischemic heart disease: comparison with Doppler echocardiography.** *J Magn Reson Imaging* 1995;5:89–92
15. Oktar SO, Yucel C, Karaosmanoglu D, et al. **Blood-flow volume quantification in internal carotid and vertebral arteries: comparison of 3 different ultrasound techniques with phase-contrast MR imaging.** *AJNR Am J Neuroradiol* 2006;27:363–69
16. Markl M, Hennig J. **Phase contrast MRI with improved temporal resolution by view sharing: k-space related velocity mapping properties.** *Magn Reson Imaging* 2001;19:669–76
17. Pruessmann KP, Weiger M, Scheidegger MB, et al. **SENSE: sensitivity encoding for fast MRI.** *Magn Reson Med* 1999;42:952–62
18. Sodickson DK, Manning WJ. **Simultaneous acquisition of spatial harmonics (SMASH): fast imaging with radiofrequency coil arrays.** *Magn Reson Med* 1997;38:591–603
19. Frayne R, Rutt BK. **Frequency response to retrospectively gated phase-contrast MR imaging: effect of interpolation.** *J Magn Reson Imaging* 1993;3:907–17